RSC Advances

PAPER

View Article Online
View Journal | View Issue

Cite this: *RSC Adv.*, 2016, **6**, 56839

Magnetic evolution of spinel $Mn_{1-x}Zn_xCr_2O_4$ single crystals

G. T. Lin,[ab] X. Luo,*[a] Q. L. Pei,[a] F. C. Chen,[ab] C. Yang,[ab] J. Y. Song,[ab] L. H. Yin,[a] W. H. Song[a] and Y. P. Sun*[acd]

Received 21st April 2016
Accepted 1st June 2016

DOI: 10.1039/c6ra10323e

www.rsc.org/advances

$Mn_{1-x}Zn_xCr_2O_4$ ($0 \leq x \leq 1$) single crystals have been grown using the chemical vapor transport (CVT) method. The crystallographic, magnetic, and thermal transport properties of the single crystals were investigated by room-temperature X-ray diffraction, magnetization $M(T)$ and specific heat $C_P(T)$ measurements. $Mn_{1-x}Zn_xCr_2O_4$ crystals show a cubic structure, the lattice constant a decreases with the increasing content x of the doped Zn^{2+} ions and follows the Vegard law. Based on the magnetization and heat capacity measurements, the magnetic evolution of $Mn_{1-x}Zn_xCr_2O_4$ crystals has been discussed. For $0 \leq x \leq 0.3$, the magnetic ground state is the coexistence of the long-range ferrimagnetic order (LFIM) and the spiral ferrimagnetic one (SFIM), which is similar to that of the parent $MnCr_2O_4$. When x changes from 0.3 to 0.8, the SFIM is progressively suppressed and spin glass-like behavior is observed. When x is above 0.8, an antiferromagnetic (AFM) order presents. At the same time, the magnetic specific heat ($C_{mag.}$) was also investigated and the results are coincident with the magnetic measurements. The possible reasons based on the disorder effect and the reduced molecular field effect induced by the substitution of Mn^{2+} ions by nonmagnetic Zn^{2+} ones in $Mn_{1-x}Zn_xCr_2O_4$ crystals have been discussed.

1 Introduction

The chalcogenide spinel compounds, named as ACr_2X_4 (A = 3d transition metals, Cd and Hg, X = O, S, Se), have attracted special interest in the past ten years because a variety of important physical effects have been found in these compounds, such as colossal magnetocapacitance (MC), multiferroicity, spin frustration and so on.[1–9] Because of the strong coupling among charge, spin and lattice degrees of freedom, ACr_2X_4 presents not only an interesting phenomena but also complicated magnetic structures.

Among ACr_2X_4 compounds, cubic spinel ACr_2O_4 oxides have special characters. The unfilled $3d^3$ shells of Cr^{3+} ions form isotropic $S = 3/2$ degree of freedom on a lattice of corner-sharing tetrahedron. When the tetrahedral A-site (A = Mg, Zn, Cd and Hg) is occupied by non-magnetic ions, the main magnetic interaction is the strong J_{CrCr} antiferromagnetic (AFM) direct exchange between the nearest-neighbor ions.[5–7] And these compounds show strongly geometrical frustration.[4,8,10–14] On the other hand, when the tetrahedral A-site is occupied by a magnetic ion, such as A = Mn, Co, Fe, and Ni, it helps to overcome the frustration of the pyrochlore lattice by the J_{ACr} coupling between the A site and the Cr^{3+} $S = 3/2$ spins.[5,15] For $MnCr_2O_4$, previous studies have calculated or evaluated from experimental data, J_{MnCr}, J_{CrCr} and J_{MnMn} and obtained that J_{CrCr} is larger than J_{MnCr} or approximately equal to J_{MnCr}.[7,16,18,24] In this case, the system presents nearly degenerated ground states and it develops complex low temperature magnetic order. Among the spinel ACr_2O_4 compounds, $MnCr_2O_4$ and $ZnCr_2O_4$ are two typical ones. In $MnCr_2O_4$, the long-range ferrimagnetic (LFIM) temperature T_C is observed around 41–51 K, which are dependent on the polycrystalline samples and single crystals. In addition, the sample exists a characteristic temperature T_S. As $T < T_S$, the long-range FIM and the short-range spiral FIM (SFIM) coexists. Between T_C and T_S, the long-range FIM with an easy axis parallel to the $\langle 110 \rangle$ direction occurs.[7,9,17–19] Very recently, the multiferroicity has also been reported in $MnCr_2O_4$ below the T_S.[9] However, $ZnCr_2O_4$ shows strikingly different characters, such as strongly geometrical frustration (the frustration factor $f \approx 31$) and high Curie–Weiss temperature $\theta = 390$–400 K. The AFM with the spin-Jahn–Teller distortion, which favors a relief of the geometrical frustration, appears around $T_N = 12$ K with the character of a first-order phase transition.[8,20,21] From above reported works, it seems to mean that the molecular field of the A sites can be effectively tuned and has the important effect on the ground state of the spinel oxides. Because the emergent phenomena present in spinel $MnCr_2O_4$ and $ZnCr_2O_4$ compounds, the magnetic evaluation of $Mn_{1-x}Zn_xCr_2O_4$ oxides are really deserved to be investigated. Although few work has

[a]*Key Laboratory of Materials Physics, Institute of Solid State Physics, Chinese Academy of Sciences, Hefei, 230031, China. E-mail: xluo@issp.ac.cn*

[b]*University of Science and Technology of China, Hefei, 230026, China*

[c]*High Magnetic Field Laboratory, Chinese Academy of Sciences, Hefei, 230031, China. E-mail: ypsun@issp.ac.cn*

[d]*Collaborative Innovation Center of Advanced Microstructures, Nanjing University, Nanjing, 210093, China*

been done on the Zn^{2+} ions doped $MnCr_2O_4$ compounds, the comprehensive study is still missing and the evolution of magnetic ground state is not very clear.[22,23] In order to further understand magnetic evolution of the ground state, herein, we investigate the effect of non-magnetic Zn^{2+} ions doping at the magnetic A sites of $Mn_{1-x}Zn_xCr_2O_4$ single crystals. The magnetic phase diagram of $Mn_{1-x}Zn_xCr_2O_4$ single crystals is obtained. We also discussed the magnetic evolution based on the disorder effect and the reduced molecular field one induced by the substitution of Mn^{2+} ions by nonmagnetic Zn^{2+} ones in $Mn_{1-x}Zn_xCr_2O_4$ crystals.

2 Experimental results

$Mn_{1-x}Zn_xCr_2O_4$ single crystals were grown by the chemical vapor transport (CVT) method, with $CrCl_3$ powders as the transport agent. Firstly, polycrystalline $Mn_{1-x}Zn_xCr_2O_4$ were made by the solid state reaction. The stoichiometric amounts of Cr_2O_3 (99%, Alfa Aesar), ZnO (99.9%, Alfa Aesar) and MnO (99%, Alfa Aesar) powders were mixed in air and sintered at 1300 °C for 20 h for several times. Powder X-ray diffraction (XRD) at room temperature revealed a single-phase without any detected impurities. Secondly, polycrystalline $Mn_{1-x}Zn_xCr_2O_4$ mixed with the $CrCl_3$ powders were ground again and sealed into several quartz tubes. All were done in the Ar-filled glove-box. All sealed quartz tubes were put in a two-zone tube furnace. The hot side is about 1060 °C and the cold side is about 1015 °C, and dwelled for 10 days, then slowly cooled down to room temperature with a rate of 15 °C h^{-1}. The crystals are octahedral with shining surfaces and the size is about 1.2 × 1.2 × 1.2 mm^3. Heat capacity was measured using the Quantum Design physical properties measurement system (PPMS-9T) and magnetic properties were performed by the magnetic property measurement system (MPMS-XL5).

3 Results and discussion

Fig. 1(a) shows the XRD pattern of $Mn_{0.8}Zn_{0.2}Cr_2O_4$ powder obtained by crushing the single crystals, which is selected as a typical sample. It also presents the structural Rietveld refinement profiles of the XRD data by the Highscore software. The refinements of the XRD data indicate that the crystals are single-phase since no extra peaks were observed. It is found that the crystals belong to the normal spinel structure and the space group is $Fd\bar{3}m$ (space group no. is 227). X-ray diffraction patterns of $Mn_{1-x}Zn_xCr_2O_4$ powder are presented in Fig. 1(b). It also presents a single-phase for all samples. The crystal structure of these samples does not change with the Zn doping content x at room temperature, the lattice parameter a decreases from 0.844 nm for $x = 0$ to 0.833 nm for $x = 1.0$, which confirms that the partial Mn^{2+} sites are occupied by the Zn^{2+} ions. The reduced lattice parameter is related to the fact that the Zn^{2+} ion radius (0.06 nm) is smaller than that of Mn^{2+} one (0.066 nm). The lattice constant a for all samples follows the Vegard law. On the other hand, these Bragg peaks of XRD pattern move towards higher angles with increasing x, which is consistent with the refined lattice parameter decreases with increasing x. Fig. 1(d) shows the enlargements of XRD pattern near the peak (511), which is selected as a typical sample.

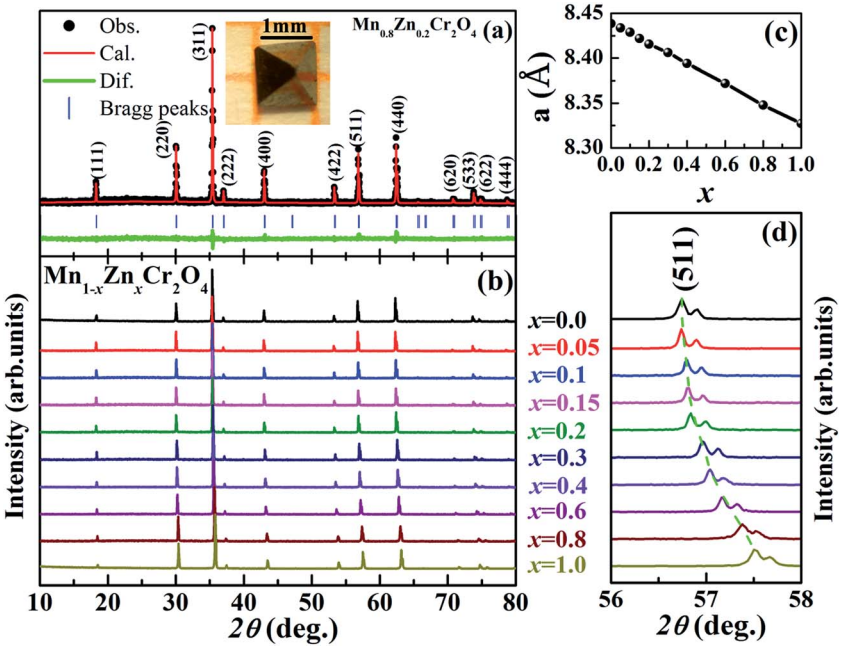

Fig. 1 (a) The refined powder XRD patterns at room temperature for the $Mn_{0.8}Zn_{0.2}Cr_2O_4$ powders crushed by single crystals. The black dots are the experimental data and the red line is the fitting result. The solid line (green line) at the bottom corresponds to the difference between experimental and calculated intensities. The blue bars are the Bragg positions. The inset shows the typical crystal of $Mn_{0.8}Zn_{0.2}Cr_2O_4$, the scale bar is 1 mm; (b) powder XRD patterns for $Mn_{1-x}Zn_xCr_2O_4$ powders crushed by the single crystals; (c) the content x of doped Zn^{2+} ions dependence of the fitted lattice parameter a; (d) the doping amount x of Zn^{2+} ions dependence of the position of Bragg peak (511).

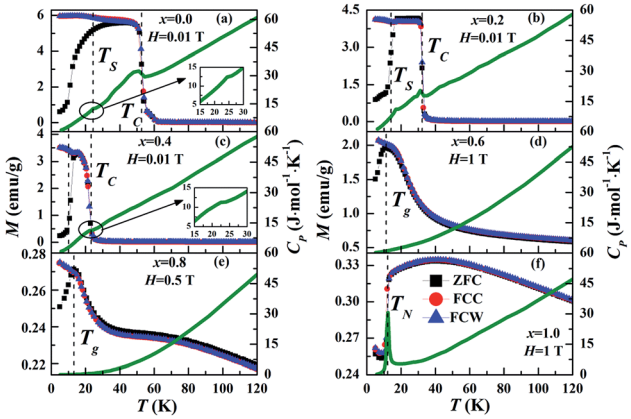

Fig. 2 (a–f) The temperature dependence of magnetization $M(T)$ and specific heat $C_P(T)$ for $Mn_{1-x}Zn_xCr_2O_4$ ($0 \le x \le 1$) single crystals. Black, red and blue lines are the magnetization measured under the ZFC, FCC and FCW modes, respectively. T_C are defined as the temperature of the minimum slope of the $M(T)$ data under the ZFC modes. Except for $MnCr_2O_4$, T_S are defined as the temperature of the maximum slope of the $M(T)$ data under the ZFC modes. T_S of $MnCr_2O_4$ is obtained from the peak of the heat capacity C_p/T. The glass freezing temperature T_g is defined as the temperature of maximum magnetization in $M-T$ curves. The olive line represents the specific heat data at $H = 0$ T. Insets of (a) and (c) present the enlarged view of the specific heat data around T_C or T_S.

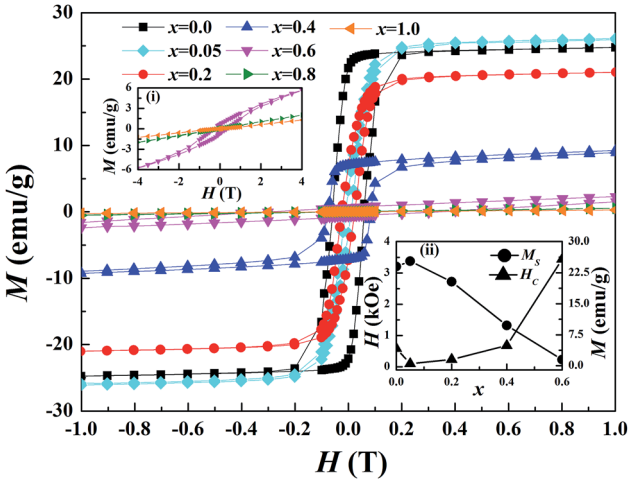

Fig. 3 The magnetic field dependence of magnetization $M(H)$ at $T = 5$ K for $Mn_{1-x}Zn_xCr_2O_4$ single crystals. The applied magnetic field is along the [111] direction. The left inset presents the enlarged view of the magnetic hysteresis loop for the doping level $x > 0.6$. The right inset shows the content x of Zn^{2+} ions dependence of the coercivity H_C and the saturation magnetization M_S for $Mn_{1-x}Zn_xCr_2O_4$ single crystals at $T = 5$ K.

In order to investigate the macroscopic magnetic properties of $Mn_{1-x}Zn_xCr_2O_4$ single crystals, we carried out the measurement of the magnetization $M(T)$ as the function of temperature. Fig. 2(a)–(f) show the $M(T)$ under the zero field-cooled (ZFC), field-cooled (FCC) and field-warming (FCW) modes with the applied magnetic field parallel to the $\langle 111 \rangle$ direction for $Mn_{1-x}Zn_xCr_2O_4$ single crystals, respectively. Fig. 2(a) and (b) show a FIM behavior for $x \le 0.2$. A collapse of the cusp is observed for the compounds with higher x in Fig. 2(c), which indicates the magnetic ground state is changed by the Zn^{2+} ion doping, namely, the SFIM may be suppressed and the magnetic ground state changes into the spin glass state in the spinel oxides.[9,24] For $x \ge 0.6$, compared with the lower doped content x, the value of the magnetization M is much smaller and the ZFC and FCC curves are obviously irreversibility in $x = 0.6$ and 0.8 (as shown in Fig. 2(d) and (e)). It may mean that both AFM and FIM orders are perturbed, then destroyed and eventually the spin-glass-like ground state presents.[24] In Fig. 2(f), accompanied by the sharp drop of magnetization $M(T)$, the AFM order occurs at $T_N = 12$ K, which is in agreement with the reported data. It is related to a structural phase transition from cubic $Fd\bar{3}m$ phase to the tetragonal $I4_1/amd$ one at T_N for $ZnCr_2O_4$.[6,25] In order to further investigate the nature of the magnetic structure of $Mn_{1-x}Zn_xCr_2O_4$ single crystals, the magnetic field dependence of the magnetization ($M(H)$) for all crystals at $T = 5$ K are shown in Fig. 3. Except for the parent $MnCr_2O_4$, it shows that the coercivity H_C increases with the increasing x for $x \le 0.6$. The saturated magnetization M_S is nearly decreasing with increasing content x.

Now we focus on the nature of Zn doped $MnCr_2O_4$ single crystals, we did the analysis on the temperature dependent inverse susceptibility $\chi^{-1}(T)$. Firstly, we pay attention to the parent compound $MnCr_2O_4$, the FIM order T_C and SFIM one T_S are 52.7 K and 24.4 K obtained from the peak of the heat capacity C_p/T, respectively. From the mean-field theory, for a AFM system and FIM one, the temperature dependent inverse susceptibility above T_C can be described by the Curie–Weiss law (eqn (1)) and the hyperbolic behavior characteristic of ferrimagnets (eqn (2)):[7,26]

$$\frac{1}{\chi} = \frac{T-\theta}{C} \quad (1)$$

$$\frac{1}{\chi_{FIM}} = \frac{T-\theta}{C} - \frac{\zeta}{T-\theta'} \quad (2)$$

where C is the Curie constant, θ is the Weiss temperature. In eqn (2), the first term is the hyperbole high-T asymptote that has a CW form and the second term is the hyperbole low-T asymptote. All the fitting results are summarized in Fig. 4(b). The substitution of Mn^{2+} ions by Zn^{2+} ions progressively perturbs the FIM structure, leading to a reduction of the effective magnetic moment μ_{eff} ($\mu_{eff} = \sqrt{3k_BC/N_A\mu_B}$) and magnetic fraction factor f ($f = \theta/T_N$) for increasing x. The tetragonal position occupied by the non-magnetic Zn^{2+} ions is responsible for the above results, which are consistent with the ones obtained from the above $M(T)$ and $M(H)$ measurements.

To study the thermal property, we performed the detailed analysis on the temperature dependent specific heat C_P/T of $Mn_{1-x}Zn_xCr_2O_4$ single crystals, as shown in Fig. 5(a). For $ZnCr_2O_4$, which yields a sharp specific heat anomaly with the character of the first-phase transition at $T_N = 12.2$ K. With the decrease of x, this heat capacity anomaly is clearly suppressed. For $0.6 \le x \le 0.8$, the heat capacity peak disappears and the specific heat presents a monotonous smooth curve, which

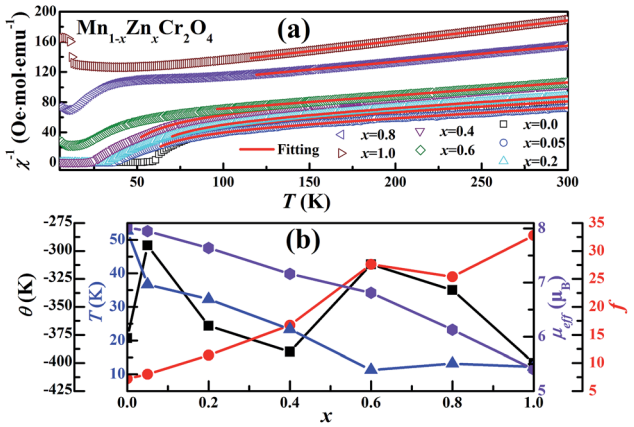

Fig. 4 (a) The inverse susceptibility dependence of the temperature for $Mn_{1-x}Zn_xCr_2O_4$ single crystals. The solid lines are the fitting results according to eqn (1) and (2); (b) the obtained effective moment μ_{eff}, Weiss temperature θ, the magnetic order temperature T (including T_C and T_N) and the frustration factor f dependence of the doping level x of the Zn^{2+} ions.

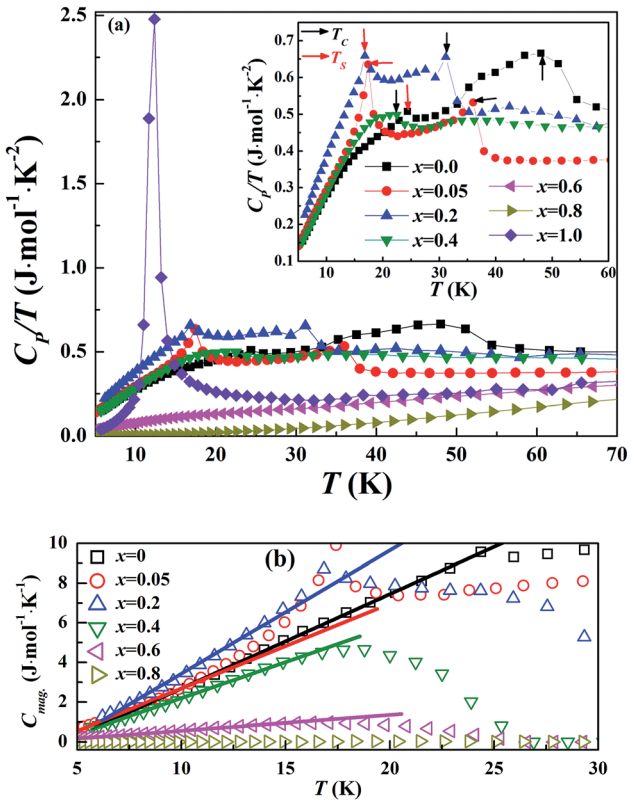

Fig. 5 (a) C_P/T curves of $Mn_{1-x}Zn_xCr_2O_4$ single crystals. The inset presents partial enlarged detail for $0 \leq x \leq 0.4$. The red and blue arrows are corresponding to T_C and T_S, respectively; (b) shows the linear dependence of magnetic specific heat $C_{mag.}$ at low temperature. The straight line guides the linear dependence.

shows a spin glass behavior.[25] It agrees well with the magnetic results. When $x \leq 0.4$, just one specific heat peak is observed, as present in the inset of Fig. 5(a), which is related to the LFIM. When x continues to decrease, two specific heat peaks are observed for $0 \leq x \leq 0.2$, and which are corresponding to the LFIM and SFIM orders. As $x \leq 0.2$, it is obvious that the magnetic structure of $Mn_{1-x}Zn_xCr_2O_4$ samples in the FIM regions is in good agreement with $MnCr_2O_4$. In addition, as shown in Fig. 5(b), the low-temperature magnetic specific heat presents linear variation in $Mn_{1-x}Zn_xCr_2O_4$. The linear variation suggests a constant density of states of the low-temperature magnetic excitations, which is claimed to be a common feature of spin glasses.[27,28] For $0.4 \leq x \leq 0.8$, a broad magnetic specific heat anomaly is observed for spin glasses, indicating that short-range-order contributions extend up to very high temperatures. Fig. 5(b) shows the temperature dependence of the magnetic heat capacity $C_{mag.}$ for $Mn_{1-x}Zn_xCr_2O_4$. Since all the samples show insulating behavior, we can ignore the electronic contribution to the heat capacity, the $C_{mag.}$ can be calculated by the following equations:[26]

$$C_{\mathrm{VDebye}}(T) = 9R\left(\frac{T}{\Theta_{\mathrm{D}}}\right)^3 \int_0^{\Theta_{\mathrm{D}}/T} \frac{x^4 e^x}{(e^x-1)^2}\,dx \quad (3)$$

$$C_{\mathrm{mag.}}(T) = C_{\mathrm{p}}(T) - nC_{\mathrm{VDebye}}(T) \quad (4)$$

where $n = 7$ is the number of atoms per formula unit, R is the molar gas constant and Θ_D is the Debye temperature. The sum of Debye functions accounts for the lattice contribution to specific heat. We can get the $C_{mag.}$ by eqn (4). We also can obtain the magnetic entropy $S_{mag.}$ from the $C_{mag.}$, which is calculated by integral of the $C_{mag.}/T$ *versus* T:[26]

$$S_{\mathrm{mag.}}(T) = \int_0^T \frac{C_{\mathrm{mag.}}(T)}{T}\,dT \quad (5)$$

The T dependence of $S_{mag.}$ is shown in Fig. 6. $S_{mag.}$ is monotonously decreasing with the increasing content x except for $ZnCr_2O_4$. In addition, the change of Debye temperature

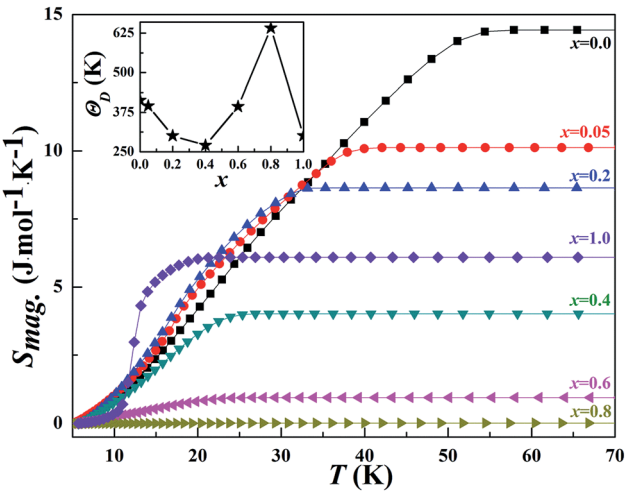

Fig. 6 The temperature dependence of the magnetic entropy $S_{mag.}$ of $Mn_{1-x}Zn_xCr_2O_4$ single crystals. The inset shows the doping content x dependence of the Debye temperature Θ_D.

behaves as firstly decreasing and then increasing with the increasing content x except for $ZnCr_2O_4$, the $x = 0.4$ sample has a minimum value $\Theta_D = 270$ K. The abnormality of $ZnCr_2O_4$ may be attributed to the character of the first-phase transition at $T_N = 12.2$ K.

Based on our obtained results, we summarize the magnetic phase diagram of $Mn_{1-x}Zn_xCr_2O_4$ single crystals as plotted in Fig. 7. Now, let us try to understand the magnetic evolution in $Mn_{1-x}Zn_xCr_2O_4$ single crystals. As we know, the substitution of Mn^{2+} ($S = 5/2$) by Zn^{2+} ($S = 0$) ions usually can induce following effects: the shrinkage of lattice, the disorder of A sites and the decreased content of magnetic Mn^{2+} ions. As shown in Fig. 2, for $x \leq 0.4$, it can be seen that all the samples undergo a transition from PM to FIM. The ZFC and FCC curves are obviously irreversibility in 0.01 T, which can be attributed to magnetic frustration or a transition into a spin-glass phase.[29–31] We note that the magnetization in 0.01 T decreases and the transition temperature T_C is lower than that of $MnCr_2O_4$ with the increase of x. Meanwhile, the FIM order presents an easy axis along the $[1\bar{1}0]$ direction in $MnCr_2O_4$ below T_C, which is identical with the axial component of Mn^{2+} ion.[7,9,18,32] Although the shrinkage of lattice could enhance the exchange interaction between Cr–Mn ions *via* oxygen 2p orbits, the decreased content of Mn ions is the major factor, which is responsible for the above observed phenomenon.[33] In $MnCr_2O_4$, the axial component of the tetrahedral A (Mn^{2+}) site is antiparallel to that of the octahedral B (Cr^{3+}) site.

According to the previous experimental evaluations and theoretical calculations, J_{CrCr} is larger than J_{MnCr} or approximately equal to J_{MnCr}.[7,16,18,24] However, as it is shown in Fig. 3, the abnormality of $MnCr_2O_4$ may be attributed to the cation distribution of A and B sites.[29] This is because Mn^{2+} site is slightly occupied by Cr^{3+} ions, which leads to the enhanced coercivity and the reduced magnetization.[34] With the substitution of magnetic ions in A site by the Zn^{2+} (has preferentially A-site occupancy), the cation distribution of A and B sites will be consistent with that of normal spinel structure. For $x \geq 0.05$, the replacement of Mn^{2+} with non-magnetic Zn^{2+} leads to the weakening of the A–O–B super exchange interaction. This would further disturb the magnetic couplings and lead to a reduction of the magnetization. The substitution of Zn^{2+} ion for Mn^{2+} or Co^{2+} ions has relatively similar physical properties. For example, Brent C Melot *et al.*[24] has reported magnetic phase evolution in the spinel compounds $Co_{1-x}Zn_xCr_2O_4$, which is similar to our results obtained in $Mn_{1-x}Zn_xCr_2O_4$. At the same time, the structure of $Co_{1-x}Zn_xCr_2O_4$ at low temperature ($T = 5$ K) is still modeled by the cubic space group $Fd\bar{3}m$ for $x \leq 0.9$.[25] For $x \geq 0.6$, the magnetic coupling interactions become more complicated. The Mn–O–Cr superexchange interaction partially breaks the spin degeneracy of the ground state and the coupling between the spin and lattice degrees of freedom becomes weaker than that of $ZnCr_2O_4$ in $Mn_{1-x}Zn_xCr_2O_4$. It is reasonable that the Mn–O–Cr superexchange interaction could disrupt the coherency of Cr–Cr exchange coupling paths, and then inhibit the spin-Jahn–Teller distortion in $Mn_{0.2}Zn_{0.8}Cr_2O_4$ and $Mn_{0.6}Zn_{0.4}Cr_2O_4$.[25] However, more detail structural experiments at low temperature, including magnetic structure determined using neutron scattering method, are needed in future.

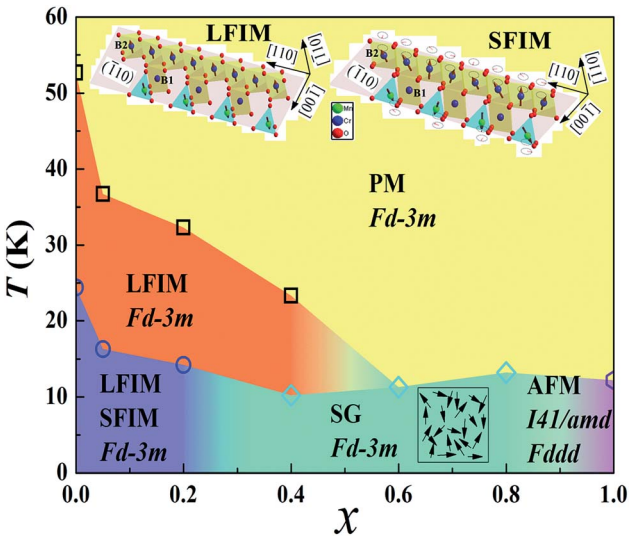

Fig. 7 The magnetic evolution of $Mn_{1-x}Zn_xCr_2O_4$ single crystals. PM, SFIM, LFIM, SG and AFM are corresponding to the paramagnetism, spiral ferrimagnetism, long-range ferrimagnetism, spin glass and antiferromagnetism, respectively.

4 Conclusion

From the room-temperature X-ray diffraction, magnetization $M(T)$ and specific heat $C_P(T)$ measurements, the crystallographic, magnetic, and thermal transport properties of the $Mn_{1-x}Zn_xCr_2O_4$ single crystals were obtained. The lattice constant a decreases with the increasing content x of the doped Zn^{2+} ions and follows the Vegard law. The magnetic evolution of $Mn_{1-x}Zn_xCr_2O_4$ crystals based on the magnetization and specific heat measurements has been discussed. For $0 \leq x \leq 0.3$, the magnetic ground state is the coexistence of LFIM and SFIM, which is similar to that of the parent $MnCr_2O_4$. x changes from 0.3 to 0.8, the SFIM is progressively suppressed and spin glass-like behavior is observed. While x is above 0.8, an AFM order presents. The magnetic specific heat ($C_{mag.}$) was also calculated and the results are coincident with the magnetic measurements. The possible reasons based on the disorder effect and the reduced molecular field effect induced by the substitution of Mn^{2+} ions by nonmagnetic Zn^{2+} ones in $Mn_{1-x}Zn_xCr_2O_4$ crystals have been discussed.

Acknowledgements

This work was supported by the Joint Funds of the National Natural Science Foundation of China and the Chinese Academy of Sciences' Large-Scale Scientific Facility under contracts U1432139, U1532152, the National Nature Science Foundation of China under contracts 51171177, 11404339, and the Nature Science Foundation of Anhui Province under contract 1508085ME103.

References

1 J. Hemberger, P. Lunkenheimer, R. Fichtl, H.-A. Krug von Nidda, V. Tsurkan and A. Loidl, *Nature*, 2005, **434**, 364–367.
2 Y. J. Choi, J. Okamoto, D. J. Huang, K. S. Chao, H. J. Lin, C. T. Chen, M. van Veenendaal, T. A. Kaplan and S.-W. Cheong, *Phys. Rev. Lett.*, 2009, **102**, 067601.
3 K. E. Sickafus, J. M. Wills and N. W. Grimes, *J. Am. Ceram. Soc.*, 1999, **82**(12), 3279–3292.
4 C. Lacroix, P. Mendels and F. Mila, Introduction to Frustrated Magnetism, in *Solid-State Sciences*, Springer Series, 2011.
5 S. Bordács, D. Varjas, I. Kézsmárki, G. Mihály, L. Baldassarre, A. Abouelsayed, C. A. Kuntscher, K. Ohgushi and Y. Tokura, *Phys. Rev. Lett.*, 2009, **103**, 077205.
6 M. C. Kemei, P. T. Barton, S. L. Moffitt, M. W. Gaultois, J. A. Kurzman, R. Seshadri, M. R. Suchomel and Y.-I. Kim, *J. Phys.: Condens. Matter*, 2013, **25**, 326001.
7 E. Winkler, S. Blanco Canosa, F. Rivadulla, M. A. López-Quintela, J. Rivas, A. Caneiro, M. T. Causa and M. Tovar, *Phys. Rev. B: Condens. Matter Mater. Phys.*, 2009, **80**, 104418.
8 S.-H. Lee, C. Broholm, W. Ratcliff, G. Gasparovic, Q. Huang, T. H. Kim and S.-W. Cheong, *Nature*, 2002, **418**, 856–858.
9 K. Dey, S. Majumdar and S. Giri, *Phys. Rev. B: Condens. Matter Mater. Phys.*, 2014, **90**, 184424.
10 M. T. Rovers, P. P. Kyriakou, H. A. Dabkowska and G. M. Luke, *Phys. Rev. B: Condens. Matter Mater. Phys.*, 2002, **66**, 174434.
11 I. Kagomiya, H. Sawa, K. Siratori, K. Kohn, M. Toki, Y. Hata and E. Kita, *Ferroelectrics*, 2002, **268**, 327–332.
12 J.-H. Chung, M. Matsuda, S.-H. Lee, K. Kakurai, H. Ueda, T. J. Sato, H. Takagi, K. P. Hong and S. Park, *Phys. Rev. Lett.*, 2005, **95**, 247204.
13 R. Valdes Aguilar, A. B. Sushkov, Y. J. Choi, S.-W. Cheong and H. D. Drew, *Phys. Rev. B: Condens. Matter Mater. Phys.*, 2008, **77**, 092412.
14 H. Ueda, H. Mitamura, T. Goto and Y. Ueda, *Phys. Rev. B: Condens. Matter Mater. Phys.*, 2006, **73**, 094415.
15 D. Tobia, J. Milano, M. Teresa Causa and E. L. Winkler, *J. Phys.: Condens. Matter*, 2015, **27**, 016003.
16 S. Blanco-Canosa, F. Rivadulla, V. Pardo, D. Baldomir, J.-S. Zhou, M. Garca-Hernndez, M. A. Lpez-Quintela, J. Rivas and J. B. Goodenough, *Phys. Rev. Lett.*, 2007, **99**, 187201.
17 J. M. Hastings and L. M. Corliss, *Phys. Rev.*, 1962, **126**, 556–565.
18 K. Tomiyasu, J. Fukunaga and H. Suzuki, *Phys. Rev. B: Condens. Matter Mater. Phys.*, 2004, **70**, 214434.
19 D. Y. Yoon, S. Lee, Y. S. Oh and K. H. Kim, *Phys. Rev. B: Condens. Matter Mater. Phys.*, 2010, **82**, 094448.
20 A. Miyata, H. Ueda, Y. Ueda, H. Sawabe and S. Takeyama, *Phys. Rev. Lett.*, 2011, **107**, 207203.
21 V. N. Glazkov, A. M. Farutin, V. Tsurkan, H.-A. Krug von Nidda and A. Loidl, *Phys. Rev. B: Condens. Matter Mater. Phys.*, 2009, **79**, 024431.
22 K. Le Dang, M. C. Mery and P. Veillet, *J. Magn. Magn. Mater.*, 1984, **43**, 161–165.
23 F. Leccabue, B. E. Watts, D. Fiorani, A. M. Testa, J. Alvarez, V. Sagredo and G. Bocelli, *J. Mater. Sci.*, 1993, **28**, 3945–3950.
24 B. C. Melot, J. E. Drewes, R. Seshadri, E. M. Stoudenmire and A. P. Ramirez, *J. Phys.: Condens. Matter*, 2009, **21**, 216007.
25 M. C. Kemei, S. L. Moffitt and L. E. Darago, *Phys. Rev. B: Condens. Matter Mater. Phys.*, 2014, **89**, 174410.
26 C. Kittle, *Introduction to Solid State Physics*, Wiley, New York, 4th edn, 1966.
27 N. P. Raju, E. Gmelin and R. K. Kremer, *Phys. Rev. B: Condens. Matter Mater. Phys.*, 1992, **46**, 5405–5411.
28 D. Meschede, F. Steglich, W. Felsch, H. Maletta and W. Zinn, *Phys. Rev. Lett.*, 1980, **44**, 102–105.
29 D. Y. Yoon, S. Lee, Y. S. Oh and K. H. Kim, *Phys. Rev. B: Condens. Matter Mater. Phys.*, 2010, **82**, 094448.
30 K. Binder and A. P. Young, *Rev. Mod. Phys.*, 1986, **58**, 801–976.
31 Z. Qu, Z. Yang, S. Tan and Y. Zhang, *Phys. Rev. B: Condens. Matter Mater. Phys.*, 2005, **71**, 184430.
32 R. Plumier, *J. Appl. Phys.*, 1968, **39**, 635–636.
33 X. Luo, Y. P. Sun, W. J. Lu, X. B. Zhu, Z. R. Yang and W. H. Song, *Appl. Phys. Lett.*, 2010, **96**, 062506.
34 A. Franco Jr and F. C. e. Silva, *J. Appl. Phys.*, 2013, **113**, 17B513.

